Research article

Network pharmacology-based analysis on the key mechanisms of Yiguanjian acting on chronic hepatitis

Xiaodan Jiang [a], Xinyi Cui [a], Ruifang Nie [a], Hongjie You [b], Zuoqing Tang [b], Wenlan Liu [a,*]

[a] *School of Traditional Chinese Medicine, Capital Medical University, Beijing, China*
[b] *School of Basic Medical Sciences, Capital Medical University, Beijing, China*

ARTICLE INFO

ABSTRACT

Chronic hepatitis (CH) encompasses a prevalent array of liver conditions that significantly contribute to global morbidity and mortality. Yiguanjian (YGJ) is a classical traditional Chinese medicine with a long history of medicinal as a treatment for CH. Although it has been reported that YGJ can reduce liver inflammation, the intricate mechanism requires further elucidation. We used network pharmacology approaches in this work, such as gene ontology (GO) analysis, Kyoto Encyclopedia of Genes and Genomes (KEGG) analysis, and network-based analysis of protein-protein interactions (PPIs), to clarify the pharmacological constituents, potential therapeutic targets, and YGJ signaling pathways associated with CH. Employing the random walk restart (RWR) algorithm, we identified GNAS, GNB1, CYP2E1, SFTPC, F2, MAPK3, PLG, SRC, HDAC1, and STAT3 as pivotal targets within the PPI network of YGJ-CH. YGJ attenuated liver inflammation and inhibited GNAS/STAT3 signaling *in vivo*. *In vitro*, we overexpressed the *GNAS* gene further to verify the critical role of GNAS in YGJ treatment. Our findings highlight GNAS/STAT3 as a promising therapeutic target for CH, providing a basis and direction for future investigations.

1. Introduction

Chronic hepatitis (CH) is a global public health concern. It features several hallmarks, such as high morbidity, high mortality, long course, and easy deterioration [1]. Hepatotoxic medications, alcohol consumption, and hepatitis virus infection are conditions that contribute to CH. It can extensively damage liver parenchymal cells, induce liver dysfunction, and eventually cause irreversible liver failure. The majority of viral infections do not cause any symptoms, but if they continue, they can cause cirrhosis, hepatocellular cancer, and other liver problems [2]. According to recent research, cirrhosis and hepatocellular carcinoma are most frequently caused by CH, and hepatocellular carcinoma is an important cause of death in patients with CH [2]. Patients with hepatocellular carcinoma often experience high rates of recurrence and metastasis post-surgery, significantly impacting their quality of life and resulting in a low five-year survival rate [3,4]. Most clinical drugs for treating hepatocellular carcinoma have not achieved good therapeutic effects, and liver transplantation is still the only effective treatment for end-stage liver disease, especially hepatocellular carcinoma. However, only 1/10,000 patients with liver disease underwent liver transplantation on time. Therefore, it is imperative to find efficient treatment approaches for treating CH to lower the number of individuals who develop hepatocellular carcinoma [5].

---

* Corresponding author.
  E-mail address: Wenlanliu1900@126.com (W. Liu).

Yiguanjian (YGJ) is a traditional Chinese medicine that dates back to the Qing Dynasty, with roots in the Treatise on Medical Cases. It comprises six botanical drugs: Shengdi, Shashen, Gouqizi, Maidong, Chuanlianzi, and Danggui. In Chinese medicine, YGJ is renowned for its ability to nourish the liver and kidney, detoxify the liver, and regulate qi. It is commonly prescribed for conditions characterized by liver and kidney yin deficiency, liver depression, and stagnation of qi. YGJ is particularly effective in alleviating liver discomforts, such as chest and epigastric dystonia, acid swallowing, and bitter vomiting, while also improving liver disorders [6]. Recent research has investigated various pharmacological effects of YGJ, which include antitumor, anti-inflammatory, antioxidant, antifibrotic, hepatoprotective, and anti-diabetic properties [7]. Following many years of use, YGJ is now accepted as an effective therapy for liver fibrosis and CH. YGJ can regulate M1/M2 macrophage polarization and treat hepatic inflammation [7].YGJ also balances metabolic disorders, regulates metabolites, such as heptaphylloside, taurine, and uric acid, and exerts anti-inflammatory and antioxidant effects to alleviate systemic inflammatory responses [8]. Clinical studies revealed that YGJ not only alleviated clinical symptoms in patients with liver disease but also reduced serum alanine transaminase (ALT) and aspartate transaminase (AST) levels. Although numerous studies have demonstrated the significant role of YGJ in reducing liver inflammation, restoring liver function, and treating CH, the precise mechanism of its action remains unclear [9,10].

Herein, we systematically examined the potential molecular mechanism of YGJ using network pharmacology to investigate how Traditional Chinese Medicine disease treatment offers numerous benefits. This approach enables a comprehensive understanding of the intricate interactions among medications, illnesses, and biological systems from a holistic perspective, mirroring the approach embraced by traditional Chinese medicine [11,12] (Fig. 1).
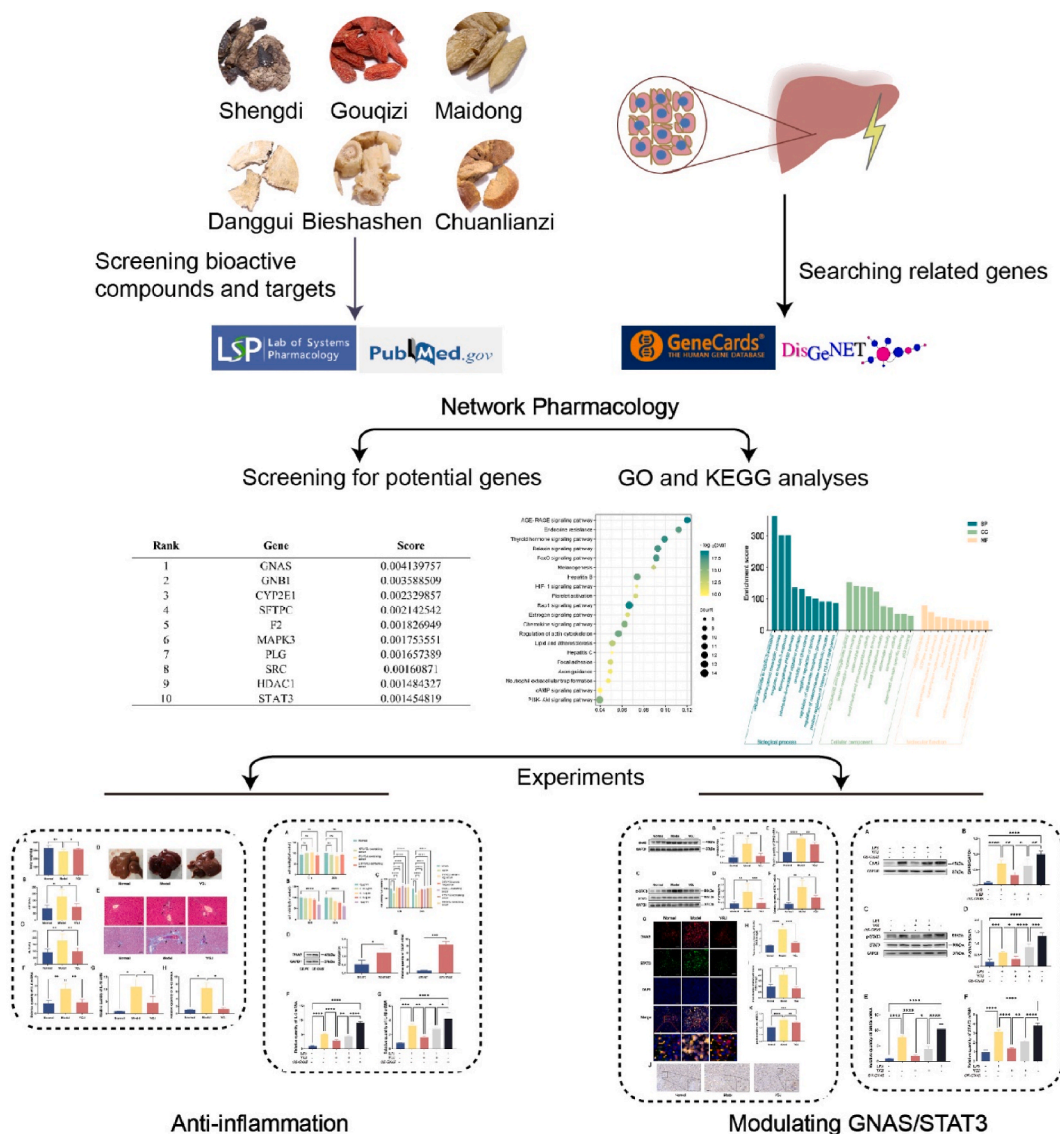

Fig. 1. Flowchart of the whole study design.

2. Methods

2.1. Gathering of active ingredients and identification of relevant targets

The Traditional Chinese Medicine Systems Pharmacology Database and Analysis Platform (TCMSP) provides absorption, distribution, metabolism, and excretion (ADME) parameters for most traditional Chinese medicines. We utilized an OB value (systemic bioavailability after oral absorption and distribution) of ≥30% and a DL value (structural similarity between compounds and clinically used medications in the DrugBank database) of ≥0.18 as screening criteria to identify the active ingredients in 4 components of YGJ: Shashen, Gouqizi, Chuanlianzi, and Danggui. We researched the active ingredients of Shengdi and Maidong in the literature, applying the same screening criteria (OB value ≥ 30% and DL value ≥ 0.18). The putative targets of the bioactive ingredients in the YGJ decoction were predicted using the TCMSP database, and 209 YGJ targets were obtained for further analysis.

2.2. Prediction of CH-related targets

We obtained disease-related genes utilizing the recently updated GeneCard database (https://www.genecards.org/) and DisGeNET (https://www.disgenet.org/), employing keywords such as "chronic hepatitis," " liver inflammation," "chronic hepatitis B," "chronic hepatitis C," "chronic hepatitis D," and "chronic hepatitis E" [13]. After removing duplicate target information, a total of 1095 unduplicated genes linked to CH were found.

2.3. Building YGJ-CH networks

We constructed a human protein interaction network comprising 11,812 nodes and 247,200 edges using the Search Tool for the Retrieval of Interacting Genes (STRING) database [14]. The STRING database gathers and consolidates all publicly accessible protein interaction network data. It aims to achieve an all-encompassing and objective network of protein interactions, including both indirect (functional) and direct (physical) interactions. STRING offers functional associations between pairs of proteins, accompanied by affinity scores that range from 0 to 1. These scores indicate the degree of confidence in protein interactions based on all available evidence, including computational predictions and experimental validation data. We established a network specifically for Homo sapiens, which only included data with an affinity score of 0.9 or higher, to guarantee the accuracy of our data. This network, referred to as the protein-protein interaction network (PPI), comprised 9941 nodes and 227,186 edges. Subsequently, we utilized the target genes of YGJ and CH diseases to build a more accurate PPI network related to YGJ-CH using Cytoscape 3.8.2.

2.4. Network-based identification of important genes in the YGJ-CH network based on YGJ targeting

Originally, Random Walks were designed to investigate a network's global topology. Particles were simulated to move repeatedly from one node to a randomly selected neighboring node [15]. Later research found that the Random Walk (RWR) algorithm could measure the affinity between the seed node and all other nodes in the network. In the algorithm, we used the restart probability (r) between a seed node and a node to denote the affinity [16]. The RWR algorithm was used to target and select important genes in the YGJ-CH network. Briefly, the YGJ-CH network was considered the core PPI network involved in the treatment of CH by YGJ. Using YGJ genes as seed genes in the core network, the RandomWalkRestartMH R package [17,18] was applied, and the "r" value was set to 0.75 [15,19,20]. The ten leading gens with the highest affinity scores for YGJ for CH were obtained and were considered the important genes for YGJ for chronic hepatitis.

2.5. Network construction and enrichment analysis

The genes with the top 50 affinity scores were selected and evaluated using Gene Ontology (GO) and Kyoto Encyclopedia of Genes and Genomes (KEGG) enrichment analyses and the DAVID Database (https://david.ncifcrf.gov/). The obtained KEGG pathway references were screened, and since cancer-related pathways would affect our CH mechanism study, we appropriately deleted some cancer-related pathways that were more intrusive to our analysis results. The results with important enrichment at a corrected p-value of <0.05 were subsequently visualized using the Microbiology Letter website (https://www.bioinformatics.com.cn/)

2.6. Yiguanjian preparation

YGJ ingredients (20 g of Shengdi, 9 g of Shashen, 9 g of Maidong, 12 g of Gouqizi, 9 g of Danggui, and 4.5 g of Chuanlianzi) were purchased from Beijing Tongrentang (Beijing, China). The YGJ mixture was soaked in distilled water for 2 h. It was then boiled and simmered for 20 min. The decoction was poured out, distilled water was added, and the mixture was simmered for another 30 min. The decoction was mixed twice and concentrated into sterile bottles with a concentration of 6.67 g/mL. Finally, the bottles were stored at 4 °C.

2.7. Animal model

A total of 27 male Wistar rats (180–200 g) were kept in a pathogen-free (SPF) environment with unrestricted access to food and

water. After a week of acclimatization feeding, the rats were randomly split into Normal (n = 9) and Model groups (n = 18). The Model group was intraperitoneally injected (i.p.) with 3 mL/kg of CCL$_4$ solution twice weekly for 8 weeks to construct the CH model. For consistency, rats in the Normal group were given the same volume of olive oil on the same schedule as Model rats. Successful modeling was judged by hematoxylin and eosin (H&E) staining of liver tissues at the end of the 8th week. CH rats with successful modeling were randomly split into the YGJ group and the Model group (n = 9/group). Rats in the YGJ group were given 6.67 g/kg YGJ once a day for 4 weeks, and equal volumes of distilled water were administered to both the Normal group and the Model group. The body surface area index values of rats and humans were used to calculate the YGJ dosage. The clinical adult YGJ decoction dosage is 63.5 g. Thus, the YGJ dose administered to the rats was calculated at 6.3 times that dose. Capital Medical University's Ethics Committee (Ethics number: AEEI-2015-123) approved the use of the experimental techniques and laboratory animals. Animal suffering was minimized during the experiment.

2.8. Sample collection

After the 12-week experimental period, the rats were anesthetized with pentobarbital sodium (25 mg/kg; i.p.). Blood was collected and left at room temperature for 60 min. Then, the serum was separated by centrifugation at 1500 g for 30 min and kept frozen at −80 °C for ALT and AST testing. The liver was removed right away, washed with pre-cooled phosphate-buffered saline (PBS), blotted clean of PBS with gauze, weighed, photographed, and preserved in liquid nitrogen and 4% paraformaldehyde. Samples preserved in liquid nitrogen were used for Western blots and Real-time quantitative PCR assays. Samples preserved in paraformaldehyde were embedded in wax blocks for Histopathological and immunohistochemical testing.

2.9. Histopathological and immunohistochemical examinations

Sections were stained with H&E and Masson's trichrome to evaluate the severity of the histological changes. Sections were also stained for immunohistochemical analysis of STAT3 protein expression. The results were visualized using a Nikon Eclipse 80i light microscope (Nikon, Tokyo, Japan). Three random fields were chosen from each group and photographed and ImageJ was used to calculate the positive areas.

2.10. Biochemical indicators of hepatic function

ALT and AST concentrations were measured using an automatic biochemical analyzer (Hitachi, Tokyo, Japan).

2.11. YGJ-containing serum preparation

A total of 20 rats were kept in an SPF setting with unlimited access to food and water. The rats were split into groups at random: YGJ and Control (n = 10/group). Rats in the YGJ group were administered YGJ suspension (6.67 g/kg) by oral gavage twice daily for 3 d, while the Control group was given the same amount of distilled water twice daily for 3 d. During the administration period, all rats were fed normally and fasted for 12 h before the last dose. One hour after the last dose, the rats were anesthetized. Blood samples were obtained from the abdominal aorta and left at room temperature for 60 min before centrifugation (1500 g for 30 min). After being collected, the serum was inactivated for 30 min at 56 °C. YGJ-containing sera and normal sera were obtained by filtration and stored at −20 °C for further in vitro experiments.

2.12. Cell culture

RAW264.7 cells were procured from Procell Life Sciences Technology (China, CL-0190). The cells were cultured adherently in Dulbecco's Modified Eagle Medium (DMEM) (Gibco, Grand Island, NY, USA) supplemented with 10% fetal bovine serum (FBS) and 1% penicillin-streptomycin solution (P/S). Passaging of cells was conducted upon reaching 80% confluence. Of note, trypsinization can induce morphological alterations in RAW264.7 cells. Therefore, during cell passaging, gentle detachment was achieved via repeated aspiration with a 5 mL pipette. Cells were then enumerated using a cell counter and passaged at a concentration of 1×10^5 cells/mL. Stable cell growth was maintained for 2–3 generations to ensure consistency for subsequent experiments.

2.13. Cell viability assay

The Cell Counting Kit-8 was used to assess the vitality of the cells (CCK-8, C6005). RAW264.7 cells were inoculated in 96-well plates and stabilized for 12 h. Subsequently, the cells were treated with varying concentrations of lipopolysaccharide (LPS; 0.01, 0.1, 0.5, and 1 µg/mL) or different concentrations of YGJ-containing serum (10% YGJ-containing serum, 5% YGJ-containing serum, and 2.5% YGJ-containing serum) for 12 and 24 h. Following treatment, the cells were washed with PBS, and the medium was discarded. After that, 10% CCK8 was added to DMEM basal media and incubated with the cells for 30 min without exposure to light. The cell culture plates were placed in an enzyme marker (BioRad, Model680, CA, USA), and the absorbance was detected at 450 nm. This was done to screen for LPS modeling conditions and assess the toxicity of YGJ-containing serum. Subsequently, using the aforementioned method, medium containing YGJ serum and LPS (1 µg/mL) was administered sequentially to screen for the optimal therapeutic concentration of YGJ-containing serum.

2.14. Cell transfection

RAW264.7 cells were divided into the OE-NC group (negative control) and the OE-GNAS group (transfected with a GNAS-overexpressing plasmid). Before transfection, the cells were suspended in DMEM medium containing 10% FBS, seeded into 6-well plates (1×10^5 cells/mL), and cultured until reaching 80% confluence. At this point, the medium was replaced with a DMEM basal medium. The cells were then transfected using Lipofectamine 2000 (11668030; Invitrogen, Carlsbad, CA, USA) with 25 μmol/mL of the plasmids (OE-NC and OE-GNAS: 5′GCAGAAGACAAGCAGGUCUATT). After 6 h of transfection, the DNEM complete medium was replaced. After 36 h, the cells were harvested, and transfection efficiency was evaluated.

2.15. Cell grouping

RAW264.7 cells were divided into 5 groups: Normal group, Model group, YGJ group, OE-GNAS + YGJ group, and OE-GNAS group. The cells in the OE-GNAS and OE-GNAS + YGJ groups were then transfected as described in section 2.14. The YGJ and OE-GNAS + YGJ groups were cultured in the presence of 5% YGJ-containing serum, while the remaining groups were cultured with normal rat serum. After 24 h, all groups except for the Normal group were stimulated with LPS (1 μg/mL) for 24 h and collected for subsequent assays.

2.16. Western blot analysis

RIPA buffer was added to liver tissues and cells and placed on ice for 20 min for lysis (Lablead, Beijing, China, CAT: P0013B), vigorously vortexed and oscillated to ensure thorough lysis, and then centrifuged at 12,000 g for 25 min to collect supernatant containing the proteins. The protein content of each supernatant was determined using the BCA protein assay and standardized to the same level by adding protein loading buffer and RIPA buffer solution. Generally, tissue protein was quantified at 6 μg/μL and cellular protein at 2 μg/μL. The proteins were denatured at 95 °C for 10 min and an equivalent quantity of sample protein was separated by 10% sodium dodecyl sulfate-polyacrylamide gel electrophoresis at 90 v. After electrophoresis, they were electrotransferred onto polyvinylidene (PVDF) membranes (Millipore, MA, USA) at 300 mA for 1.5 h. The PVDF membrane was then incubated for 1 h in 5% skimmed milk.

Primary antibodies were prepared in 5% skimmed milk, and the cut PVDF membranes were individually incubated with specific primary antibodies at 4 °C overnight. Subsequently, the membranes were incubated with anti-rabbit IgG (1:5000 Jackson Immuno Research, PA, USA, CAT: 312-005-003) or anti-mouse IgG-HRP (1:5000 Proteintech, Wuhan, China, CAT: SA00001-1) for 2 h. The blots were then imaged using an Image Lab system (Bio-Rad ChemiDoc XRS, CA, USA), and Western blots were densitometrically analyzed with ImageJ software. Protein expression levels were compared with GAPDH internal reference proteins to determine differences in expression. All experiments were conducted in triplicate.

The following primary antibodies were used: GNAS (1:1000 Abcam, USA, CAT: 283266), Phospho-STAT3 (1:1000 Cell Signaling Technology, USA, CAT: 9145), Phospho-STAT3 (1:2000 Abcam, USA, CAT: ab76315), STAT3 (1:1000 Cell Signaling Technology, USA, CAT: 9139), and GAPDH (1:5000 Proteintech, China, CAT: 60004-1-Ig-100UL).

2.17. Real-time quantitative PCR analysis

TRIzol reagent (TaKaRa, Beijing, China) was added to liver tissues and cells and vortexed with shaking for 20 min to extract total RNA. Chloroform was added at a ratio of 1:5 (chloroform to TRIzol reagent) to isolate RNA. Then, isopropanol was added to precipitate the RNA, and it was purified by adding 75% ethanol. Finally, the extracted total RNA was dissolved in 20 μL of DEPC-treated water. The concentration and purity of RNA were determined spectrophotometrically according to the A260/A280 ratio, which was expected to be in the range of 1.8–2.0. For mRNA detection, 5000 ng of total RNA was reverse-transcribed to complementary DNA (cDNA) using the Reverse Transcription Kit (Servicebio, Wuhan, China, CAT: G3337). The reaction consisted of 4 μL of 5 × SweScript All-in-One SuperMix for qPCR, 1 μL gDNA Remover, total RNA, and surplus double-distilled H_2O_2 in a 20 μL reaction volume. Next, qPCR was

Table 1
Primer sequences.

Primer name	Sequences 5′–3′
GAPDH-F	CTGGAGAAACCTGCCAAGTATG
GAPDH-R	GGTGGAAGAATGGGAGTTGCT
GNAS-F	GTCCTCGCTGGGAAATCG
GNAS-R	CCACGGCGCAGGTAAAGT
STAT3-F	TTAGGGCCTGGTGTGAACTAC
STAT3-R	CATGATGTACCCTTCATTCCA
IL-6-F	CAACGCTGCTGGGAGTCTTGT
IL-6-R	GACAAGGCTTTTTGTTGTTTGCTTC
IL-Iβ-F	GCCCATCCTCTGTGAC TCAT
IL-Iβ-R	AGGCCACAGGTATTTTGT
IL-I8-F	GCCTGTGTTCGAGGA TATGACT
IL-I8-R	CCTTCACAGAGAGGGTCACAG

performed using the SYBR Green Taq kit (Servicebio, Wuhan, China, CAT: G3320) on a 7500HT Fast Real-time PCR system. The reaction consisted of 10 μL of 5 × SYBR Green qPCR Mix, 0.4 μL of forward primer (10 μM), 0.4 μL of reverse primer (10 μM), cDNA, and surplus double-distilled H_2O_2 in a 20 μL reaction volume. The PCR assay was conducted under the following conditions: 1) 30 s at 95 °C, and 2) 40 cycles of 20 s at 95 °C, 20 s at 60 °C, and 20 s at 72 °C. Four replicate wells were set up for each gene and repeated 3 times. Gene expression was quantified by the comparative Ct method (ΔΔCt), and the relative expressions were calculated using the $2^{-\Delta\Delta Ct}$ method. The specific primers for qRT-PCR are shown in Table 1.

2.18. Immunofluorescence staining

The paraffin sections were sequentially deparaffinized in xylene and various concentrations of ethanol. Subsequently, the sections were blocked with 10% normal goat serum for 1 h, followed by overnight incubation at 4 °C with anti-GNAS antibody (1:500, Abcam, Cambridge, MA, UK, CAT: 283266) and anti-STAT3 antibody (1:200, Cell Signaling Technology, USA, CAT: 9139). After washing with PBS, the sections were incubated with CY3-conjugated goat anti-rabbit IgG (H + L) (1:300, Servicebio, Wuhan, CAT: GB21303) and 488-conjugated goat anti-mouse IgG (H + L) (1:300, Servicebio, Wuhan, CAT: GB25301) for 2 h. The sections were coated with an antifade mounting medium containing 4',6-diamidino-2-phenylindole (DAPI) and examined with a Nikon Ti2–U fluorescence microscope (Nikon Instruments, Wetzlar, Japan). Three random fields were selected and photographed, and the fluorescence intensity was analyzed using ImageJ.
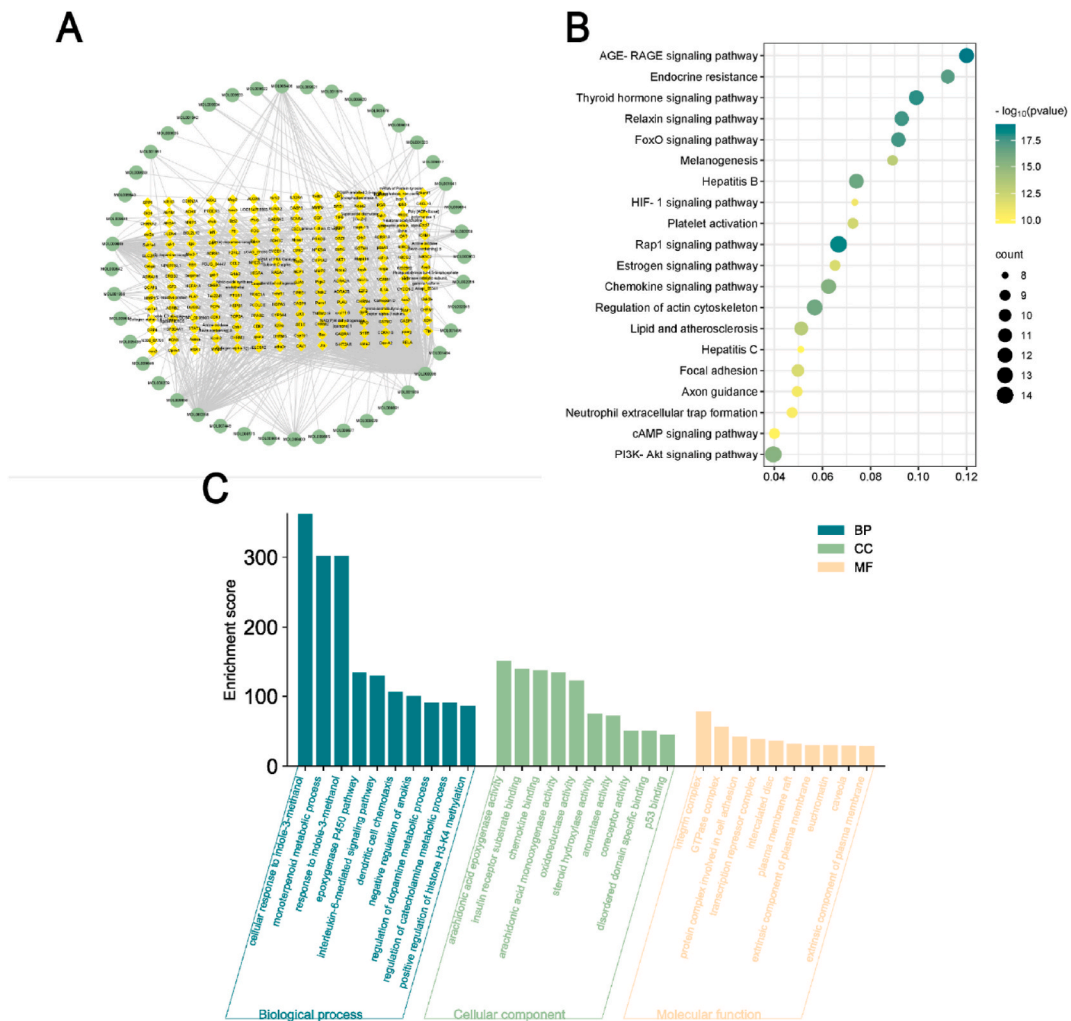

Fig. 2. Compounds in YGJ and their corresponding targets. (A) YGJ Compound-target network. Potential genes-based analysis: (B) KEGG pathways, (C) biological processes (BPs), cellular components (CCs), and molecular functions (MFs).
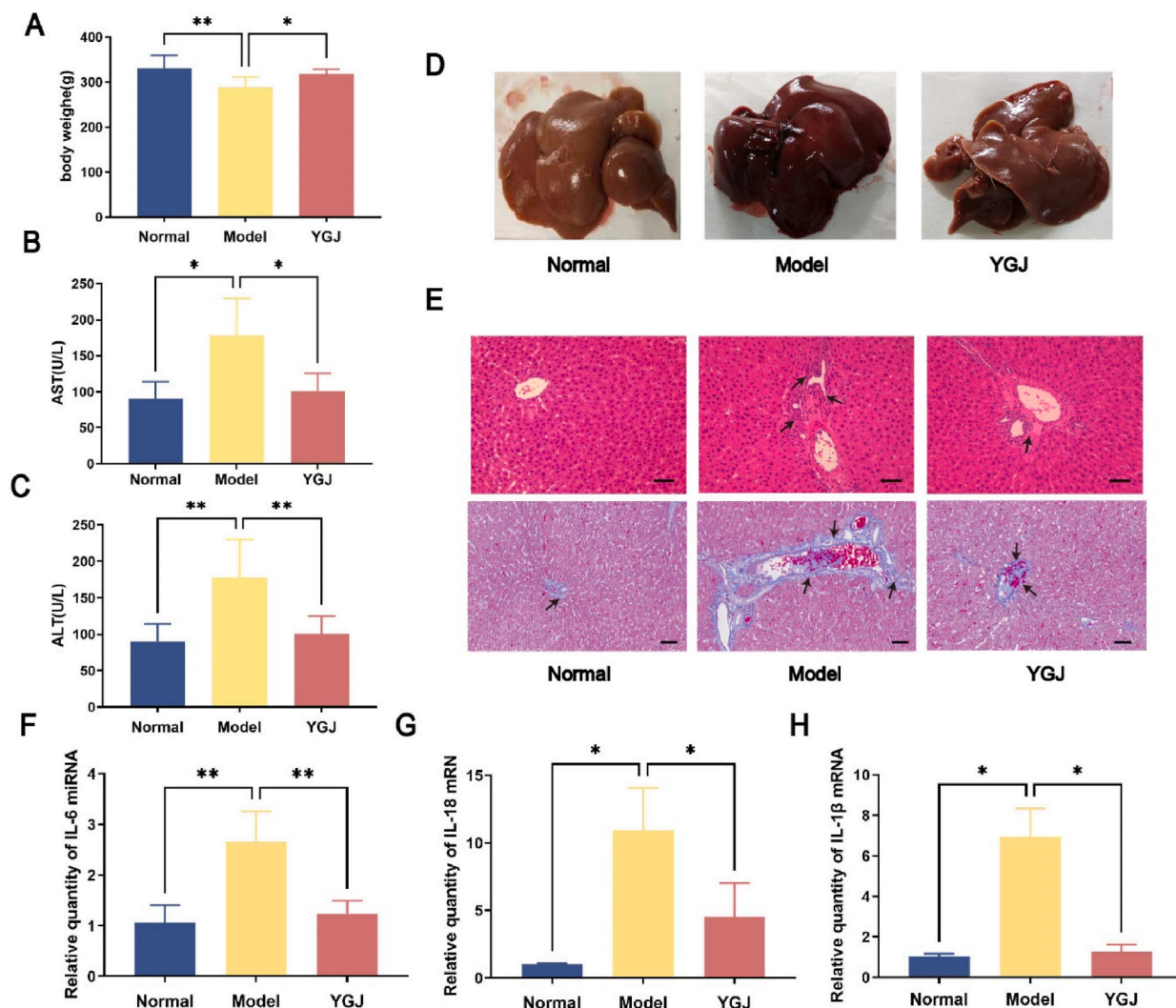
Fig. 3. YGJ improved liver function and reduced hepatic inflammation. (A) Body weight measurement. (B) Serum ALT level. (C) Serum AST level. (D) Morphology of the liver in each group. (E) Representative images of H&E and Masson-stained liver tissue (original magnification, × 200; scale bars, 50 μm). (F) Liver interleukin 6 (IL-6) levels. (G) Liver interleukin 18 (IL-18) levels. (H) Liver interleukin 1β (IL-1β) levels. Data represent the mean ± SD (n = 3); $*p < 0.05$, $**p < 0.01$.

2.19. Statistical analysis

All data are expressed as means ± SD. The Student's t-test was utilized for statistical comparisons between any 2 groups, while one-way ANOVA and Dunnett's multiple comparison test were used for comparisons among multiple groups. GraphPad Prism 9 was used to generate all bar plots. *P-values of < 0.05* indicated statistically significant differences.

3. Results

3.1. YGJ compounds and targets

A total of 44 unduplicated compounds and 209 unduplicated targets of YGJ were found, and distributed among 5 locations in Shengdi, 8 in Shashen, 35 in Gouqizi, 5 in Maidong, 2 in Danggui, and 6 in Chuanlianzi. Gouqizi was identified as the botanical drug with the highest contribution ratio to the collected compounds and targets (Fig. 2A).

3.2. CH-related genes and YGJ-CH network

A total of 1095 disease genes for CH were predicted using the online database, and a YGJ-CH subnetwork was constructed based on
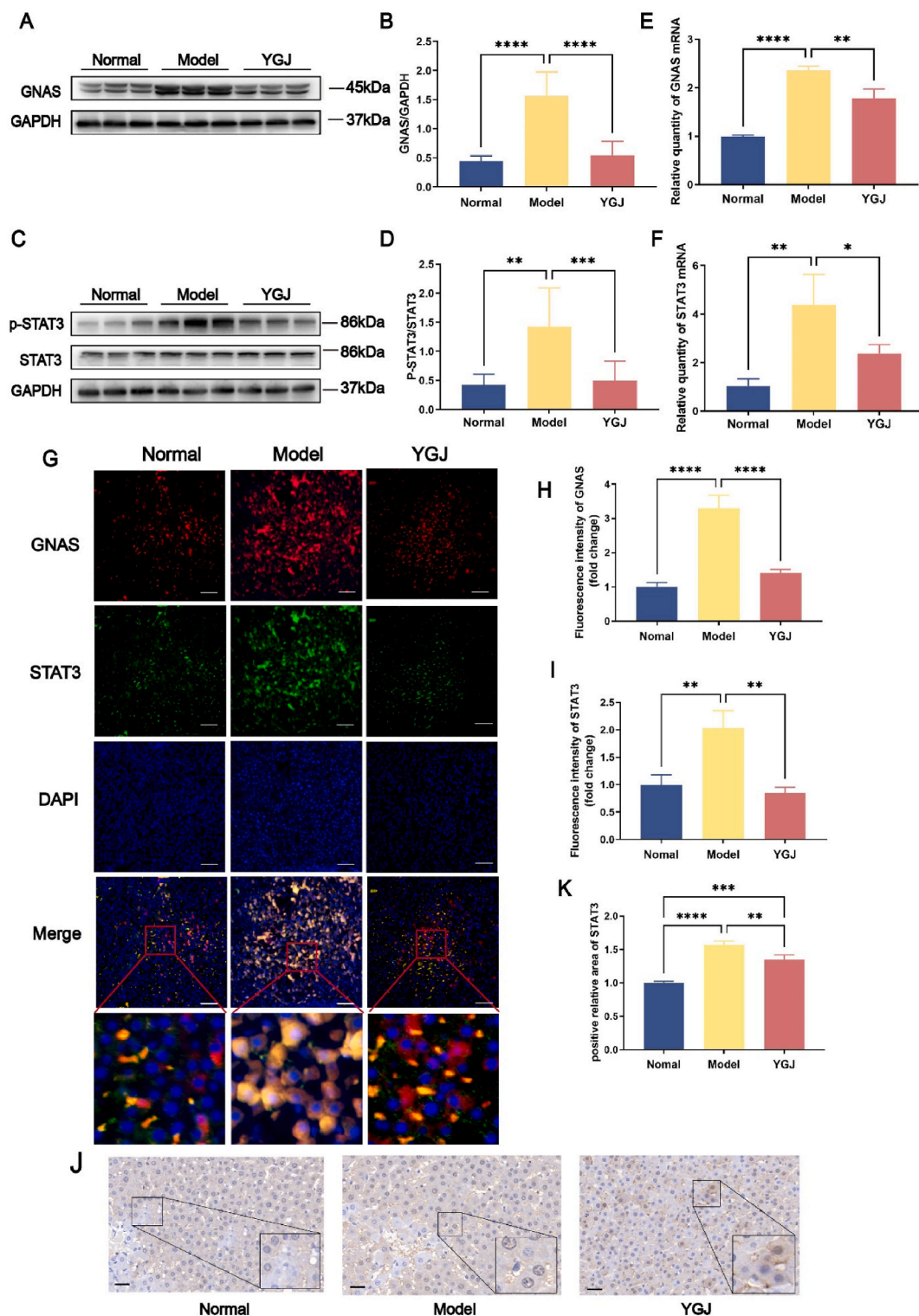
Fig. 4. YGJ inhibited GNAS/STAT3 signaling in CH. (A) Expressions of GNAS determined by Western Blot (See Supplementary Material 4A for unadjusted strips). (B) Quantitative analysis of the GNAS/GAPDH expression ratio. (C) Expression of signal transducer and activator of transcription (STAT3) and phosphorylated STAT3 (p-STAT3) determined by Western Blot (See Supplementary Material 4C for unadjusted strips). (D) Quantitative analysis of the p-STAT3/STAT3 expression ratio. (E–F) Quantification of GNAS and STAT3 mRNA by qRT-PCR. (G) The expression of GNAS and STAT3 in the liver tissues of each group was determined by immunofluorescence (original magnification, × 400; scale bar = 10 μm). A region is boxed randomly in each group and the boxed regions are further enlarged below (magnification, × 1600). (H–I) Quantitative analysis of the GNAS

and STAT3 fluorescence intensity. (J) The representative photomicrographs of immunohistochemistry staining of STAT3 in paraffin-embedded liver samples (original magnification, $\times$ 400; scale bars= 25 μm). (K) Quantitative analysis of the STAT3 positive relative area. Data represent the mean $\pm$ SD (n = 3); $*p < 0.05$, $**p < 0.01$, $***p < 0.001$, $****p < 0.0001$.

the PPI network, containing 1998 nodes and 17,435 interactions.

3.3. Prediction of the key CH-related genes by the RWR algorithm

Using the YGJ seed genes as a basis, RWR analysis was conducted on the PPI network to determine affinity scores and identify the important genes in CH. As shown in Table 2, the approach yielded the top 10 genes (*GNAS, GNB1, CYP2E1*, SFTPC, *F2, MAPK3, PLG, SRC, HDAC1*, and *STAT3*) as hub genes. GNAS is a frequently mutated gene in human cancers; mutations in this gene are seen in many different types of cancer, including liver, lung, pancreatic, and rectal cancers [21–25]. Elevated GNAS expression induces inflammation-associated hepatocellular carcinoma progression and poor prognosis. GNAS induces hepatic inflammation by activating STAT3 via IL-6/STAT3 [26,27]. STAT3 inhibition reduces the release of interleukin (IL)-17 and exerts anti-inflammatory and hepatoprotective effects [28]. The active ingredient of YGJ, quercetin, exerts anti-inflammatory effects by inhibiting STAT3 polarization and increasing macrophage polarization to the M2 phenotype [29].

Therefore, based on the results of the RWR analysis, we speculated that YGJ could exert a therapeutic effect in CH via GNAS/STAT3. The biological functions and enriched signaling pathways of these genes were then investigated by GO and KEGG analyses. From the top 20 pathways identified by KEGG enrichment analysis, we retrieved a total of 6 signaling pathways related to liver diseases as core pathways (Rap1, PI3K-Akt, AGE-RAGE, FoxO, and hepatitis B) (Fig. 2B). The Rap1 signaling pathway can effectively regulate the inflammatory response. Rap1A can enhance nuclear factor (NF)-κB activity through AGE/RAGE signaling, resulting in increased tumor necrosis factor (TNF)-α expression and the generation of free radicals, thereby promoting inflammation [30]. The PI3K-AKT signaling pathway is essential to regulating metabolism, protein synthesis, and inflammation, as well as influencing cell proliferation, division, and autophagy. Research has demonstrated a close association between activation of the PI3K/AKT pathway and inflammation in acetaminophen-induced liver injury [17]. Additionally, CD73 has been found to inhibit the activation of the inflammasome, suppress hepatocyte apoptosis, and attenuate steatohepatitis through the PI3K/AKT signaling pathway [18]. AGE is associated with liver function and liver injury [31]. Oxidative stress and inflammation brought on by AGEs can exacerbate liver damage. AGEs negatively impact the polarization and anti-inflammatory functions of M2 macrophages [32] while promoting the pro-inflammatory response of M1 macrophages. They activate the RAGE receptor initiating multiple signaling pathways, including PKC, PI3K/Akt, JAK/STAT, and MAPK/ERK. Activation of these intrinsic pathways subsequently triggers other transcription factors such as NF-κB and Egr-1, leading to the upregulation of inflammation, oxidative damage, and alterations in cell motility, adhesion, and metabolism, ultimately resulting in tissue damage [33]. GO analysis indicated that the potential targets were focused on the level of organic matter and lipid metabolism in biological progression, oxidoreductase activity in molecular function, and plasma membrane levels in cellular components (Fig. 2C).

3.4. YGJ attenuates liver injury in CH rats

The therapeutic effect of YGJ was investigated using a carbon tetrachloride (CCL$_4$)-induced CH rat model. Significant changes in rat body weight were seen after CCL$_4$ and YGJ interventions. The results showed that CCL$_4$ intervention reduced the body weight of the rats, and YGJ treatment prevented this, which contributed to weight gain in the CH rats (Fig. 3A). YGJ not only affected the body weight of the CH model rats but also the serum AST and ALT levels, which are indicators of liver injury. YGJ reversed CCL$_4$-induced increases in serum ALT and AST (Fig. 3B–C). Observation of the rat livers revealed distinct differences among the groups. In comparison to the Normal group, the livers in the Model group exhibited a dark red color, rough surfaces with varying-sized granules, and adhesions between liver lobes. Occasional adhesions were also observed between the liver surface and the thoracic diaphragm. However, significant changes were observed in the YGJ group. The livers appeared light red, with smooth and soft surfaces and reduced adhesions between liver lobes (Fig. 3D). These findings collectively indicate that YGJ has the potential to ameliorate CCL$_4$-induced liver injury.

Table 2
Top 10 genes ranked by RWR analysis.

Rank	Gene	Score
1	GNAS	0.004139757
2	GNB1	0.003588509
3	CYP2E1	0.002329857
4	SFTPC	0.002142542
5	F2	0.001826949
6	MAPK3	0.001753551
7	PLG	0.001647389
8	SRC	0.00160871
9	HDAC1	0.001484327
10	STAT3	0.001454819

3.5. YGJ reduces hepatic inflammation in CH rats

H&E staining revealed distinct histological differences in the liver tissues of the rats across the groups. In the Normal group, hepatocytes exhibited an orderly arrangement, with intact hepatic lobular structures and nuclei. Only a few cells showed signs of inflammatory infiltration. Conversely, the Model group displayed a disorganized hepatocyte arrangement, disrupted hepatic lobular structures, extensive inflammatory cell infiltration, and hepatocyte necrosis. However, in the YGJ group, there was a notable improvement in hepatocyte arrangement, with reduced cell necrosis and inflammatory infiltration compared to the Model group. Masson staining demonstrated variations in collagen deposition within the liver tissues. Minimal collagen deposition was observed in the Normal group, with occasional scattered collagen among the hepatocytes. In contrast, the Model group exhibited widespread collagen deposition throughout the hepatic tissues. However, in the YGJ group, there was less collagen deposition (Fig. 3E).

The pathologic studies showed overall higher tissue injury scores in the Model groups compared to the Normal group (Tables 3 and 4). The injury score for the YGJ group was lower than that of the Model group ($P < 0.01$). We examined the expression of various inflammatory cytokines in different groups to investigate the impact of YGJ on mitigating liver inflammation (Fig. 3F–H). qRT-PCR analysis revealed that IL-6 expression was increased in liver tissues after CCL$_4$ stimulation compared to the Normal group. However, IL-6 levels decreased significantly following treatment with YGJ. Similar trends were observed for other inflammatory factors, such as IL-18 and IL-1β, indicating the effectiveness of YGJ in alleviating inflammation in the rat model of CH.

3.6. YGJ inhibits GNAS/STAT3 signaling in CH rats

We then evaluated the potential effects of YGJ on the GNAS and STAT3 signaling pathways in different groups (Fig. 4A–D). Western blot analysis showed that, compared to the Normal group, the Model group exhibited elevated GNAS protein expression, with no notable change in STAT3 protein expression, whereas the level of p-STAT3 protein was markedly higher. Conversely, compared to the Model group, the YGJ group demonstrated markedly reduced GNAS protein expression and decreased levels of p-STAT3 protein. These findings suggest that YGJ may regulate the *GNAS* gene and influence the activation of its downstream genes, thereby mitigating liver inflammation. The qRT-PCR analysis results were consistent with the Western blot analysis. The relative expression of miRNAs for *GNAS* and *STAT3* was increased in the Model group and decreased in the YGJ group (Fig. 4E–F). The same results were also demonstrated by immunofluorescence and immunohistochemistry. The immunofluorescence findings revealed that, relative to the Normal group, the fluorescence intensity of GNAS and STAT3 was notably augmented in the Model group. However, following YGJ treatment, the fluorescence intensity of both GNAS and STAT3 exhibited a decrease. Interestingly, GNAS and STAT3 displayed synchronized changes in fluorescence intensity, suggesting a correlation between the 2 proteins (Fig. 4G–I). The immunohistochemical results revealed a marked rise in the STAT3-positive area in the Model group compared to the Normal group. However, in the YGJ group, there was a notable decrease in the STAT3-positive area. Both fluorescence intensity and positive area served as reliable indicators of target protein expression (Fig. 4J–K). Collectively, all results indicated that YGJ improved liver injury and suppressed hepatic inflammation through GNAS/STAT3 signaling in CH rats.

3.7. Effect of YGJ-containing serum on RAW264.7 cell viability and inflammation

Next, we evaluated the ability of YGJ to repress inflammation in vitro and investigated the related mechanisms. The CCK-8 assay was used to evaluate the viability of RAW264.7 cells incubated in YGJ-containing serum for 12 h and 24 h. Compared with the control group, no reduction in cell viability was observed in the YGJ-containing serum-treated groups, suggesting that YGJ-containing serum was not cytotoxic (Fig. 5A). We examined the effect of varying concentrations of LPS (0.01, 0.1, 0.5, 1 mg/mL) on cell viability at different points (12 h and 24 h) to determine the optimal concentration for modeling the inflammatory stimulation of RAW264.7 cells. At 24 h, a significant decrease in the viability cell cultured treated with LPS at 1 μg/mL was observed (Fig. 5B). Therefore, this concentration was chosen as the modeling concentration for use in later research. The cell viability of the LPS-stimulated group decreased, whereas that of the YGJ-containing serum groups increased (Fig. 5C). The most significant increase was observed in the 5% YGJ-containing serum group. Therefore, that concentration was chosen as the treatment dose for use in subsequent studies.

3.8. YGJ-containing serum reduces LPS-induced inflammation in RAW264.7 cells

We generated GNAS-overexpressing RAW264.7 cells to further investigate whether YGJ attenuated the expression of inflammatory factors by regulating GNAS gene expression. Western blot and qRT-PCR analyses confirmed that *GNAS* was highly expressed at both the protein and mRNA levels in cells transfected with the OE-GNAS plasmid but not in cells transfected with the OE-NC control

Table 3
The criteria for liver tissue histopathology assessment.

Criterion	Description
Lobular Inflammation	The severity relative to the Standard Control (grade 0) group graded (0–3)
Hepatocyte Death	Hepatocyte death graded (0–3) based on the percentage of hepatocyte deaths
Lobules of liver	The severity relative to the Standard Control (grade 0) group graded (0–3)
hepatic fibrosis	Hepatic fibrosis graded (0–3) based on the percentage of collagen area

Table 4
Histopathological assessment of liver.

Criterion	Group		
	Normal	Model	YGJ
Lobular Inflammation	0.5	1.5	1
Hepatocyte Death	0	0	0
Lobules of liver	0.4	1.2	0.7
hepatic fibrosis	0.5	1.4	0.8
Total liver tissue injury score	1.4	4.1***	2.5**

Histopathologic injury scores in mice at the 12th week. ***$P < 0.001$, in comparison with Normal group. **$P < 0.01$, in comparison with Model group.

(Fig. 5D–E). The inflammatory factor assay revealed that LPS significantly elevated the expression of IL-6 compared to the Normal group. Transfection with OE-GNAS further heightened the expression of IL-6. However, treatment with YGJ attenuated the elevated expression of IL-6 induced by LPS and OE-GNAS. Similar results were observed for the inflammatory factor IL-1β. These findings suggest that both LPS stimulation and GNAS overexpression can induce cellular inflammation, whereas YGJ treatment effectively reduces the expression of inflammatory factors, indicating its therapeutic potential in treating inflammation. (Fig. 5F–G).

3.9. YGJ reduces inflammation by inhibiting GNAS and suppressing activation of the GNAS/STAT3 pathway

Next, we explored the effects of YGJ on GNAS and STAT3 signaling in vitro. The Western blot results showed that LPS and OE-GNAS stimulation increased GNAS protein expression and STAT3 activation, and YGJ decreased GNAS expression and inhibited STAT3 activation. (Fig. 6A–D). qRT-PCR analysis revealed that the expression of the *GNAS* and *STAT3* genes was significantly increased in the LPS and OE-GNAS groups. Notably, the levels of GNAS and STAT3 were decreased in the YGJ and YGJ + OE-GNAS groups (Fig. 6E–F). All these results suggest that YGJ reduced inflammation by inhibiting the GNAS/STAT3 signaling pathway and that GNAS is particularly important.

4. Discussion

CH is a liver disease with high morbidity and mortality rates. It has been increasing globally and poses a significant threat to public health [34]. Especially in the Asia-Pacific region, CH is a major cause of cirrhosis and hepatocellular carcinoma [35]. Given that severe cirrhosis and hepatocellular carcinoma are irreversible conditions, the aggressive treatment of CH becomes particularly crucial to retard disease progression. While therapeutic drugs commonly employed in clinical practice, such as interferon and entecavir, exert definite antiviral effects, they may also have certain side effects and prove costly, thereby amplifying the financial burden on patients. Traditional Chinese medicine, in contrast, has demonstrated superior efficacy in the treatment of CH, with minimal side effects and a favorable safety profile. Hence, it holds promise as a potential therapeutic option for CH. A substantial body of clinical and experimental research has confirmed the beneficial effects of YGJ. It not only improves symptoms and safeguards liver function but also diminishes liver injury while regulating collagen metabolism in liver tissue. YGJ has been widely used in the treatment of chronic liver diseases, including CH, liver fibrosis, and cirrhosis. YGJ has been shown to effectively address chronic liver injury by targeting the MAPK/NF-κB pathway [9]. It regulates the Wnt signaling pathway to suppress astrocyte activation, thereby mitigating liver fibrosis and impeding cirrhosis progression [10]. Recent findings indicated that YGJ reduced hepatic inflammation by inhibiting M1 macrophage polarization [7].

Previous studies have employed a network pharmacology strategy to explore the mechanism behind the benefits of YGJ in treating chronic liver disease. However, the mechanism in CH remains unclear. Our study represents an innovative extension of previous research into the direct targets of YGJ in the treatment of chronic liver disease. Unlike previous studies, we employed the Whole Human Protein Database to explore the potential targets of YGJ for treating CH in a broader context. Our hypothesis was that YGJ potentially targets nearby targets in addition to direct targets in treating CH. We focused more on neighboring targets and introduced the RWR algorithm to identify important genes through RWR scores. Based on the RWR rankings, GNAS was identified as the most significant target for CH treatment with YGJ. GNAS is closely linked with various malignancies, such as liver cancer, colorectal cancer [36], lung cancer [37], and biliary tract cancer [38]. Within this research, we verified that YGJ reduced GNAS expression and inhibited STAT3 activation, thus reducing the inflammatory response. We also showed that YGJ can reduce inflammation in CH, indicating that this treatment may prevent progression to liver cancer. Compound screening in the search for targets and pharmacodynamic analysis facilitated a comprehensive exploration of the therapeutic benefits of YGJ for CH, thereby opening up new avenues for the treatment of CH and the prevention of liver cancer.

TCMSP screening of YGJ compounds and the experimental validation showed that the decoction contained a variety of pharmacological constituents, such as quercetin, Kaempferol, Rhodiola, β-sitosterol, and dousterol, that can reduce inflammation and have therapeutic effects on CH. Recent research showed that quercetin reduced liver inflammation and fibrosis by modulating M1 macrophage polarization [39]. Kaempferol was found to mitigate oxidative stress and inflammation by suppressing the NF-κB/p65 and Nrf2/HO-1 pathways [40]. It treats CH by attenuating HBsAg and HBeAg, activating caspase-3, and down-regulating the PI3K-Akt signaling pathway [41]. Rhodiola rosea glycosides have been shown to decrease creatinine enzyme levels and regulate
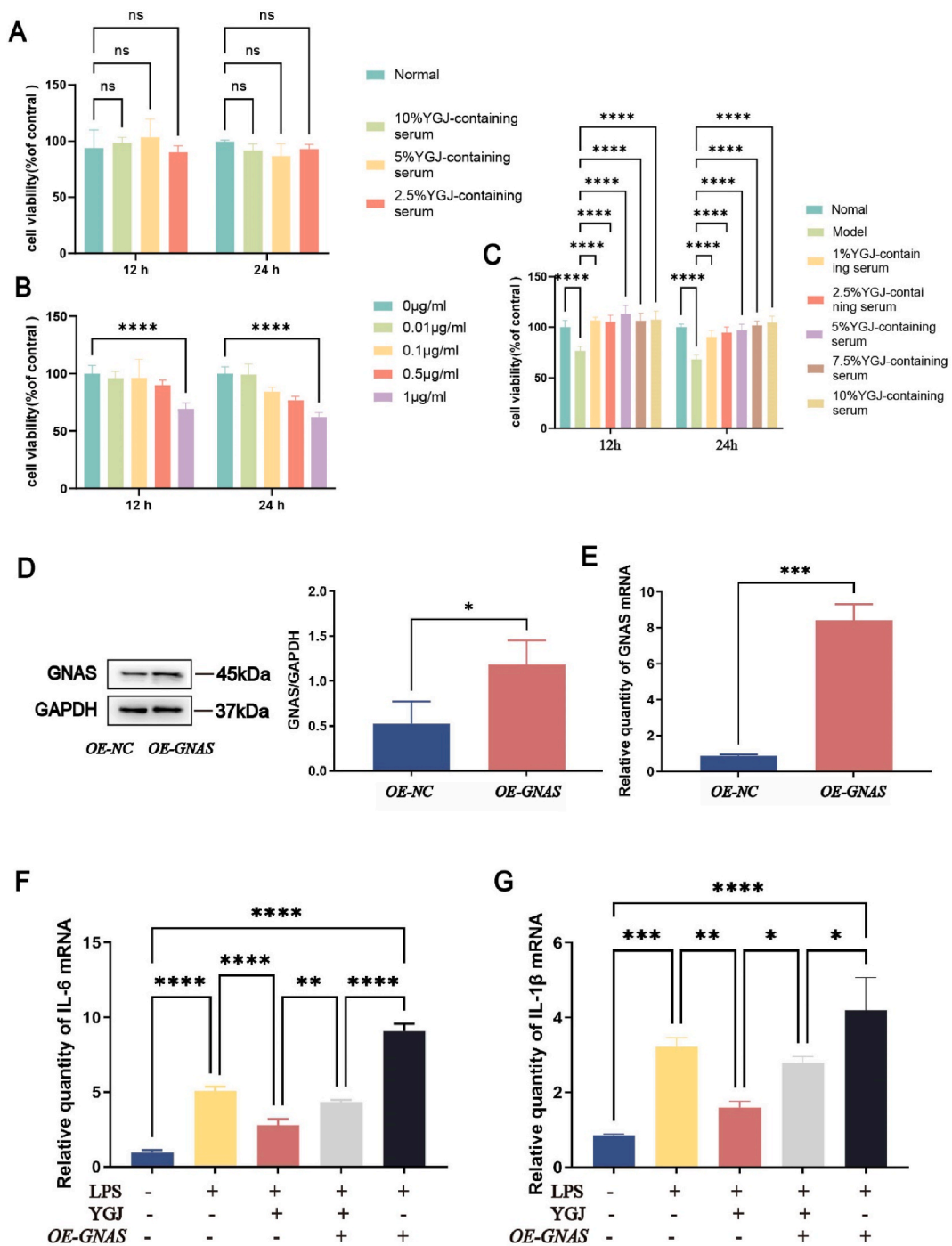
Fig. 5. Effect of YGJ-containing serum on RAW264.7 cell viability and inflammation. (A) Effect of YGJ-containing serum on the viability of RAW264.7 cells. (B) Effects of LPS on the viability of RAW264.7 cells. (C) Effects of YGJ-containing serum on the viability of RAW264.7 cells after LPS stimulation. (D–E) Western Blot and qRT-PCR analyses of the OE-GNAS transfection efficiency (See Supplementary Material 5D for unadjusted strips). (F–G) Quantification of IL-6 and IL-1β mRNA determined by qRT-PCR. Data represent the mean ± SD (n = 3); *$p < 0.05$, **$p < 0.01$, ***$p < 0.001$, ****$p < 0.0001$.

inflammatory responses in serum. Additionally, they possess potent free radical scavenging abilities and aid in the treatment of furan-induced hepatocellular injury. Rhodiola rosea glycosides were also shown to exert hepatoprotective properties by inhibiting the anti-inflammatory and antioxidant activation of the SIRT1/NF-κB pathway and NLRP3 inflammatory vesicles [42]. Both β-sitosterol and stigmasterol can induce the apoptosis of human hepatocarcinoma cells and significantly increase cellular reactive oxygen species
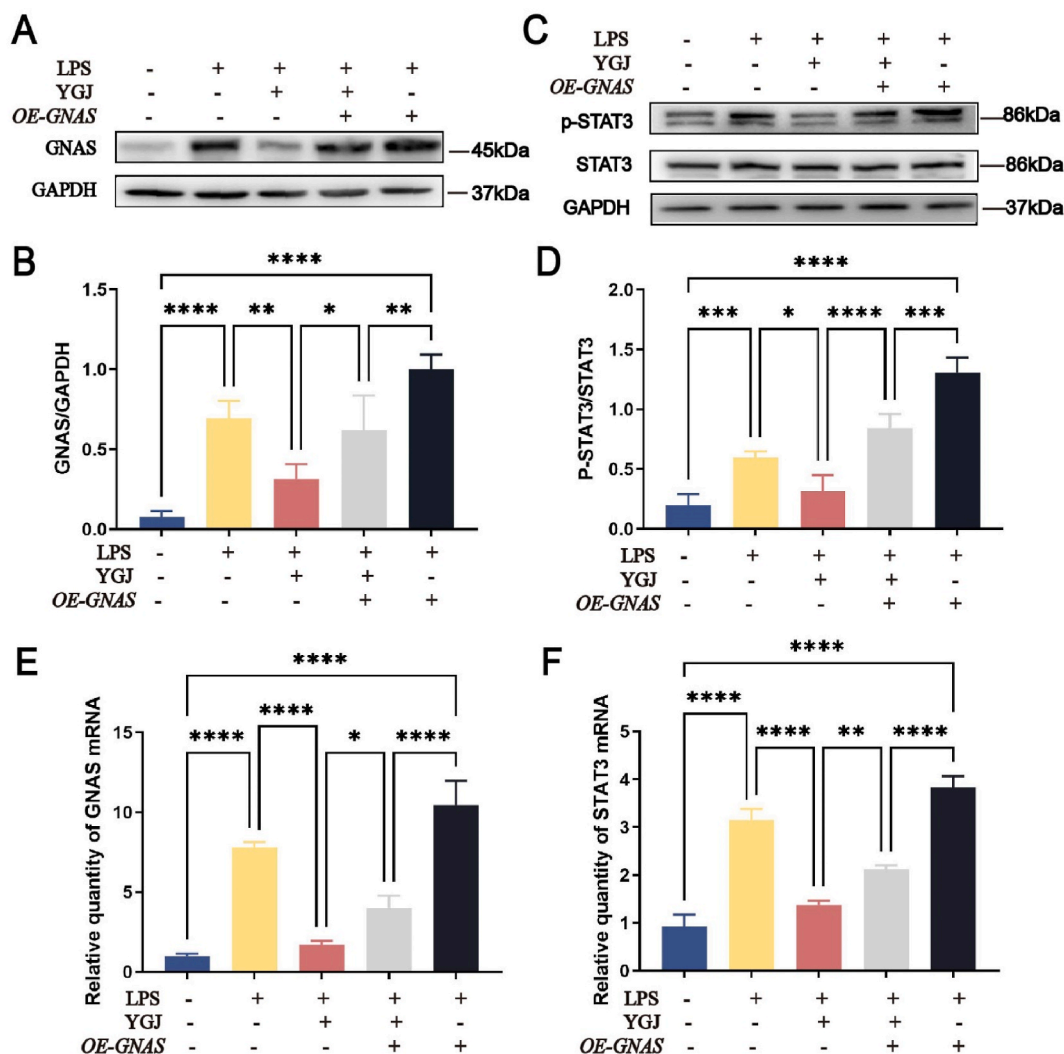
Fig. 6. YGJ-containing serum inhibited GNAS/STAT3 signaling in LPS-stimulated RAW264.7 cells. (A) Expression of GNAS determined by Western Blot (See Supplementary Material 6A for unadjusted strips). (B) Quantitative analysis of the GNAS/GAPDH expression ratio. (C) Expression of signal transducer and activator of transcription (STAT3) and phosphorylated STAT3 (p-STAT3) determined by Western Blot (See Supplementary Material 6C for unadjusted strips). (D) Quantitative analysis of the p-STAT3/STAT3 expression ratio. (E–F) Quantification of GNAS and STAT3 mRNA determined by qRT-PCR. Data represent the mean $\pm$ SD (n = 3); *$p < 0.05$, **$p < 0.01$, ****$p < 0.0001$.

and Ca^{2+} levels [43].

KEGG and GO analysis were performed to explore the roles of the predicted YGJ targets. GO analysis indicated that the potential targets were primarily enriched in organic matter and lipid metabolism within the biological process category, oxidoreductase activity within the molecular function category, and plasma membrane within the cellular components category. In addition, the KEGG findings were related to the CH pathway. After screening out cancer-related pathways and excluding the interference of cancer pathways on the results, we retrieved a total of 6 signaling pathways related to liver diseases as core pathways (Rap1, PI3K-Akt, AGE-RAGE, FoxO, and hepatitis B), all of which have been connected to chronic inflammation [44–47].

Based on the RWR rankings, the leading 10 targets were *GNAS, GNB1, CYP2E1, SFTPC, F2, MAPK3, PLG, SRC, HDAC1,* and *STAT3*. *GNAS* encodes the alpha-subunit of the stimulatory G protein (Gsα), which produces cAMP to control the release of neurotransmitters and other hormones [6,48,49]. Some studies also indicated that GNAS mutations are closely associated with inflammation-associated liver cancer [26]. Mechanistically, the loss of GNAS blocks the activation of STAT3 to suppress the inflammatory response of hepatocellular carcinoma cells [27]. STAT3 interacts with a variety of signals and has significant functions in liver inflammation. Above all, STAT3 plays a central role in multiple KEGG pathways, including the AGE-RAGE [50], FoxO [51], PI3K-Akt [51], and hepatitis B signaling pathways.

Experiments using animal models are crucial for evaluating the effectiveness of TCM. We investigated the mechanism underlying the therapeutic effects of YGJ in CCL$_4$-induced liver inflammation [52]. H&E staining allows for the assessment of liver inflammation.

According to the pathological data, CCl$_4$ caused inflammation and liver damage in the Model group. However, YGJ successfully stopped these pathological alterations. Serum ALT and AST are also closely connected with liver damage and liver function, serving as indicators of inflammation and liver injury. Serum ALT and AST levels were much lower in the YGJ-treated group than in the Model group. All data indicated that YGJ effectively alleviated CCl$_4$-induced liver injury and inflammation. In addition, the expression of inflammatory factors, which directly reflect the degree of inflammation, was significantly reduced after YGJ treatment. Our results suggest that YGJ treatment can reduce inflammation and restore liver function. We tested the screened genes and pathways to further explore the mechanism. The experimental data indicated that YGJ treatment reduced GNA protein expression and inhibited STAT3 activation.

Cellular tests were conducted to better understand the therapeutic mechanism of traditional Chinese medicine. LPS is commonly used to establish a cellular model of inflammation. We investigated the effect of YGJ-containing serum to reduce inflammation induced by LPS and OE-GNAS in RAW264.7 cells. The results showed that the expression of inflammatory factors was lower in both the YGJ and OE-GNAS + YGJ groups compared with the Model and OE-GNAS groups and was higher in the OE-GNAS + YGJ group than in the YGJ group. The mechanism may be linked to the downregulation of GNAS expression. For further validation, we explored YGJ effects on the GNAS/STAT3 pathway. The experimental results showed that YGJ-containing serum reduced GNAS protein expression and STAT3 activation in both the Model and OE-GNAS groups, and the effect was more marked in the YGJ group than in the OE-GNAS + YGJ group. These results were confirmed at the gene expression level by qRT-PCR analysis. Thus, our study suggests that GNAS/STAT3 plays a pivotal role in liver inflammation, highlighting GNAS as a potential therapeutic target for CH. The investigation into the GNAS/STAT3 pathway and the pivotal GNAS target has illuminated fresh perspectives for comprehending the initiation and advancement of CH, presenting innovative therapeutic targets for its management. Leveraging this focal point, prospective diagnostic and therapeutic methodologies can be devised for clinical application. This inquiry assists in elucidating novel mechanisms underlying CH pathogenesis, facilitating prompt clinical interventions for CH, and presenting avenues and tactics for mitigating "inflammation-cancer" metamorphosis correlated with CH. The study also elucidated the mechanism by which YGJ treats CH and provides considerations for YGJ's therapeutic potential in various diseases through its action on GNAS, thereby expanding the clinical applications of YGJ.

5. Conclusions

In conclusion, the pharmacological constituents, potential therapeutic targets, and related signaling pathways of YGJ in treating CH were revealed by a network pharmacology system and RWR algorithm and validated. Our study suggested that the GNAS/STAT3 pathway may serve as a potential mechanism for treating CH and preventing liver cancer, with GNAS identified as a key target (Fig. 7a-c). This breakthrough offers valuable insight for future CH investigations and expands the clinical utility of YGJ. However, our study had some limitations. Network pharmacology is constrained and supported by existing public databases. Thus, any bias in these data will limit the predictive accuracy of the network pharmacology analysis. In future research related to network pharmacology, we should enhance the quality control of the databases, regularly update data, and promptly reflect the latest research developments. Additionally, integrating data from multiple databases for comprehensive analysis is crucial. Emphasizing experimental validation and conducting in-depth validation whenever possible should be the focus of our studies.

Ethical approval

Every procedure involving experimental animals was carried out strictly in compliance with Capital Medical University's Ethics Committee guidelines. The number of approvals is AEEI-2015-123.

Consent

The permission to participate and publish is not relevant.

Data availability statement

Most data are provided in the Supplementary Material of the article. Additional data and analytical methods in the current work can be obtained from the corresponding authors.

CRediT authorship contribution statement

Xiaodan Jiang: Writing – original draft, Visualization, Validation, Methodology, Conceptualization. **Xinyi Cui:** Methodology, Data curation. **Ruifang Nie:** Writing – review & editing, Supervision, Data curation. **Hongjie You:** Writing – review & editing. **Zuoqing Tang:** Writing – review & editing, Supervision. **Wenlan Liu:** Writing – review & editing, Resources, Investigation, Funding acquisition, Conceptualization.
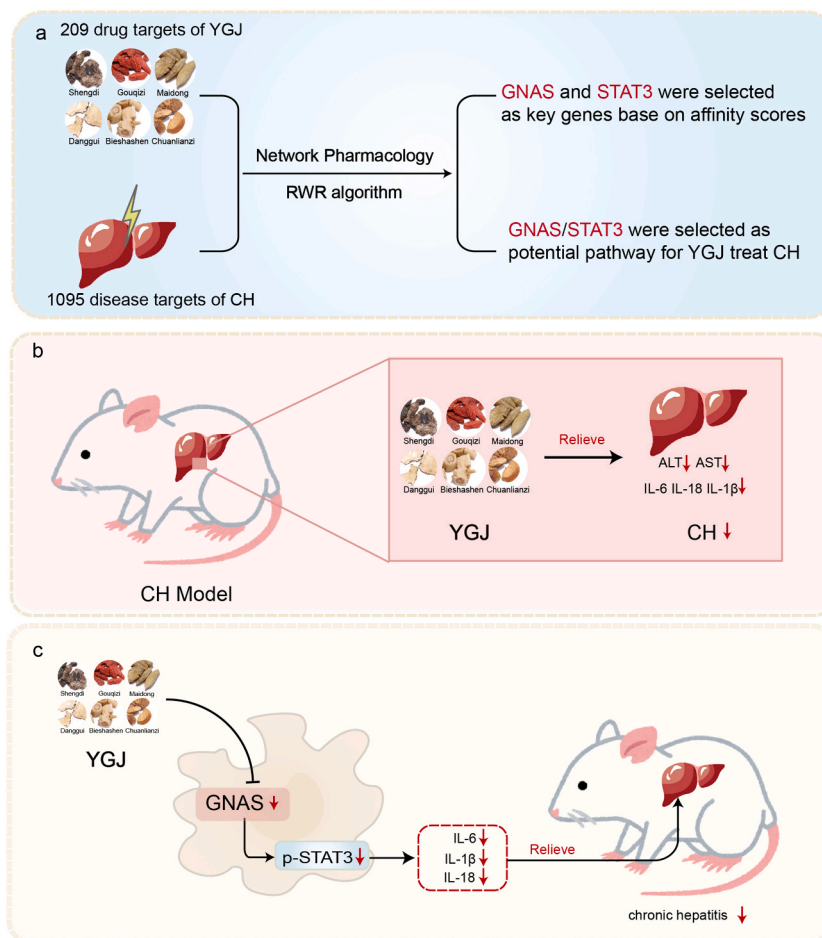
Fig. 7. Schematic diagram of the mechanism of YGJ treatment of CH. (a) Screening YGJ for important genes in the treatment of chronic hepatitis. (b) YGJ alleviates liver injury to treat CH. (c) YGJ alleviates inflammation and treats CH via the GNAS/STAT3 signaling pathway.

Declaration of competing interest

The author(s) declared no potential conflicts of interest with respect to the research, authorship, and/or publication of this article.

Appendix A. Supplementary data

Supplementary data to this article can be found online at https://doi.org/10.1016/j.heliyon.2024.e29977.

References

[1] W.J. Jeng, G.V. Papatheodoridis, A.S.F. Lok, Hepatitis B, Lancet 401 (2023) 1039–1052, https://doi.org/10.1016/S0140-6736(22)01468-4.
[2] A.G. Singal, E. Zhang, M. Narasimman, N.E. Rich, A.K. Waljee, Y. Hoshida, et al., HCC surveillance improves early detection, curative treatment receipt, and survival in patients with cirrhosis: a meta-analysis, J. Hepatol. 77 (2022) 128–139, https://doi.org/10.1016/j.jhep.2022.01.023.
[3] P. Liu, L. Kong, Y. Liu, G. Li, J. Xie, X. Lu, A key driver to promote HCC: cellular crosstalk in tumor microenvironment, Front. Oncol. 13 (2023) 1135122, https://doi.org/10.3389/fonc.2023.1135122.
[4] A.J. Craig, J. von Felden, T. Garcia-Lezana, S. Sarcognato, A. Villanueva, Tumour evolution in hepatocellular carcinoma, Nat. Rev. Gastroenterol. Hepatol. 17 (2020) 139–152, https://doi.org/10.1038/s41575-019-0229-4.

[5] A. Tu, X. Zhu, P.Z. Dastjerdi, Y. Yin, M. Peng, D. Zheng, et al., Evaluate the clinical efficacy of traditional Chinese Medicine as the neoadjuvant treatment in reducing the incidence of hepatocellular carcinoma in patients with hepatitis B-related cirrhosis: a systematic review and meta-analysis, Heliyon 10 (2024) e24437, https://doi.org/10.1016/j.heliyon.2024.e24437.

[6] C. Lu, S. Zhang, S.S. Lei, D. Wang, B. Peng, R. Shi, et al., A comprehensive review of the classical prescription Yiguan Jian: phytochemistry, quality control, clinical applications, pharmacology, and safety profile, J. Ethnopharmacol. 319 (2024) 117230, https://doi.org/10.1016/j.jep.2023.117230.

[7] Y. Xu, W. Xu, W. Liu, G. Chen, S. Jiang, J. Chen, et al., Yiguanjian decoction inhibits macrophage M1 polarization and attenuates hepatic fibrosis induced by CCl (4)/2-AAF, Pharm. Biol. 59 (2021) 1150–1160, https://doi.org/10.1080/13880209.2021.1961820.

[8] M. Yin, D. Zhou, F. Jia, X. Su, X. Li, R. Sun, et al., Metabolomics analysis of the potential mechanism of Yi-Guan-Jian decoction to reverse bone loss in glucocorticoid-induced osteoporosis, J. Orthop. Surg. Res. 18 (2023) 409, https://doi.org/10.1186/s13018-023-03778-6.

[9] X. Lixin, G. Erli, H. Songping, Z. Yonggen, J. Wang, Y. Lijun, Yi Guan Jian, a Traditional Chinese Herbal Medicine, Alleviates carbon tetrachloride-induced liver injury, Evid Based Complement Alternat Med 2019 (2019) 9824728, https://doi.org/10.1155/2019/9824728.

[10] Y. Xu, W.W. Fan, W. Xu, S.L. Jiang, G.F. Chen, C. Liu, et al., Yiguanjian decoction enhances fetal liver stem/progenitor cell-mediated repair of liver cirrhosis through regulation of macrophage activation state, World J. Gastroenterol. 24 (2018) 4759–4772, https://doi.org/10.3748/wjg.v24.i42.4759.

[11] J.F. Liu, A.N. Hu, J.F. Zan, P. Wang, Q.Y. You, A.H. Tan, Network pharmacology deciphering mechanisms of volatiles of wendan granule for the treatment of alzheimer's disease, Evid Based Complement Alternat Med 2019 (2019) 7826769, https://doi.org/10.1155/2019/7826769.

[12] B. Niu, H. Zhang, C. Li, F. Yan, Y. Song, G. Hai, et al., Network pharmacology study on the active components of Pterocypsela elata and the mechanism of their effect against cerebral ischemia, Drug Des. Dev. Ther. 13 (2019) 3009–3019, https://doi.org/10.2147/DDDT.S207955.

[13] J. Pinero, J.M. Ramirez-Anguita, J. Sauch-Pitarch, F. Ronzano, E. Centeno, F. Sanz, et al., The DisGeNET knowledge platform for disease genomics: 2019 update, Nucleic Acids Res. 48 (2020) D845–D855, https://doi.org/10.1093/nar/gkz1021.

[14] D. Szklarczyk, A.L. Gable, D. Lyon, A. Junge, S. Wyder, J. Huerta-Cepas, et al., STRING v11: protein-protein association networks with increased coverage, supporting functional discovery in genome-wide experimental datasets, Nucleic Acids Res. 47 (2019) D607–D613, https://doi.org/10.1093/nar/gky1131.

[15] A. Valdeolivas, L. Tichit, C. Navarro, S. Perrin, G. Odelin, N. Levy, et al., Random walk with restart on multiplex and heterogeneous biological networks, Bioinformatics 35 (2019) 497–505, https://doi.org/10.1093/bioinformatics/bty637.

[16] D. Smedley, S. Kohler, J.C. Czeschik, J. Amberger, C. Bocchini, A. Hamosh, et al., Walking the interactome for candidate prioritization in exome sequencing studies of Mendelian diseases, Bioinformatics 30 (2014) 3215–3222, https://doi.org/10.1093/bioinformatics/btu508.

[17] J. Xia, L. Lv, B. Liu, S. Wang, S. Zhang, Z. Wu, et al., Akkermansia muciniphila ameliorates acetaminophen-induced liver injury by regulating gut microbial composition and metabolism, Microbiol. Spectr. 10 (2022) e0159621, https://doi.org/10.1128/spectrum.01596-21.

[18] H. Zhu, M. Zhang, Y. Ye, Z. Liu, J. Wang, X. Wu, et al., CD73 mitigates hepatic damage in alcoholic steatohepatitis by regulating PI3K/AKT-mediated hepatocyte pyroptosis, Biochem. Pharmacol. 215 (2023) 115753, https://doi.org/10.1016/j.bcp.2023.115753.

[19] J. Yang, S. Tian, J. Zhao, W. Zhang, Exploring the mechanism of TCM formulae in the treatment of different types of coronary heart disease by network pharmacology and machining learning, Pharmacol. Res. 159 (2020) 105034, https://doi.org/10.1016/j.phrs.2020.105034.

[20] X. Wei, W. Hou, J. Liang, P. Fang, B. Dou, Z. Wang, et al., Network pharmacology-based analysis on the potential biological mechanisms of sinisan against non-alcoholic fatty liver disease, Front. Pharmacol. 12 (2021) 693701, https://doi.org/10.3389/fphar.2021.693701.

[21] M. Hsu, M. Sasaki, S. Igarashi, Y. Sato, Y. Nakanuma, KRAS and GNAS mutations and p53 overexpression in biliary intraepithelial neoplasia and intrahepatic cholangiocarcinomas, Cancer 119 (2013) 1669–1674, https://doi.org/10.1002/cncr.27955.

[22] B.M. Walther, I. Walther, Y. Chen, I. Petersen, GNAS1 mutation analysis in gastrointestinal tumors, Folia Histochem. Cytobiol. 52 (2014) 90–95, https://doi.org/10.5603/FHC.2014.0011.

[23] R. Rao, R. Salloum, M. Xin, Q.R. Lu, The G protein Galphas acts as a tumor suppressor in sonic hedgehog signaling-driven tumorigenesis, Cell Cycle 15 (2016) 1325–1330, https://doi.org/10.1080/15384101.2016.1164371.

[24] L.L. Ritterhouse, M. Vivero, M. Mino-Kenudson, L.M. Sholl, A.J. Iafrate, V. Nardi, et al., GNAS mutations in primary mucinous and non-mucinous lung adenocarcinomas, Mod. Pathol. 30 (2017) 1720–1727, https://doi.org/10.1038/modpathol.2017.88.

[25] T. Hata, M. Mizuma, F. Motoi, Y. Omori, M. Ishida, K. Nakagawa, et al., GNAS mutation detection in circulating cell-free DNA is a specific predictor for intraductal papillary mucinous neoplasms of the pancreas, especially for intestinal subtype, Sci. Rep. 10 (2020) 17761, https://doi.org/10.1038/s41598-020-74868-2.

[26] J.C. Nault, M. Fabre, G. Couchy, C. Pilati, E. Jeannot, J. Tran Van Nhieu, et al., GNAS-activating mutations define a rare subgroup of inflammatory liver tumors characterized by STAT3 activation, J. Hepatol. 56 (2012) 184–191, https://doi.org/10.1016/j.jhep.2011.07.018.

[27] H. Ding, X. Zhang, Y. Su, C. Jia, C. Dai, GNAS promotes inflammation-related hepatocellular carcinoma progression by promoting STAT3 activation, Cell. Mol. Biol. Lett. 25 (2020) 8, https://doi.org/10.1186/s11658-020-00204-1.

[28] D. Li, J. Chen, B. Lin, Y. Guo, J. Pan, C. Yu, et al., Celastrol pretreatment attenuates concanavalin A-induced hepatitis in mice by suppressing interleukin-6/STAT3-interleukin-17 signaling, J. Gastroenterol. Hepatol. 38 (2023) 821–829, https://doi.org/10.1111/jgh.16183.

[29] Y. Zou, J. Jiang, Y. Li, X. Ding, F. Fang, L. Chen, Quercetin regulates microglia M1/M2 polarization and alleviates retinal inflammation via ERK/STAT3 pathway, Inflammation (2024), https://doi.org/10.1007/s10753-024-01997-5.

[30] S.D. Burr, J.A. Stewart Jr., Rap1a overlaps the AGE/RAGE signaling cascade to alter expression of alpha-SMA, p-NF-kappaB, and p-PKC-zeta in cardiac fibroblasts isolated from type 2 diabetic mice, Cells 10 (2021), https://doi.org/10.3390/cells10030557.

[31] S.A. Palma-Duran, M.D. Kontogianni, A. Vlassopoulos, S. Zhao, A. Margariti, M. Georgoulis, et al., Serum levels of advanced glycation end-products (AGEs) and the decoy soluble receptor for AGEs (sRAGE) can identify non-alcoholic fatty liver disease in age-, sex- and BMI-matched normo-glycemic adults, Metabolism 83 (2018) 120–127, https://doi.org/10.1016/j.metabol.2018.01.023.

[32] Q. Wang, G. Zhu, X. Cao, J. Dong, F. Song, Y. Niu, Blocking AGE-RAGE signaling improved functional disorders of macrophages in diabetic wound, J. Diabetes Res. 2017 (2017) 1428537, https://doi.org/10.1155/2017/1428537.

[33] Correction to: 2016 ATVB plenary lecture: receptor for advanced glycation endproducts and implications for the pathogenesis and treatment of cardiometabolic disorders: spotlight on the macrophage, Arterioscler. Thromb. Vasc. Biol. 37 (2017) e66, https://doi.org/10.1161/ATV.0000000000000057.

[34] P.O. Collaborators, Global prevalence, treatment, and prevention of hepatitis B virus infection in 2016: a modelling study, The Lancet Gastroenterology & Hepatology 3 (2018).

[35] M.C.S. Wong, J.L.W. Huang, J. George, J. Huang, C. Leung, M. Eslam, et al., The changing epidemiology of liver diseases in the Asia-Pacific region, Nat. Rev. Gastroenterol. Hepatol. 16 (2019) 57–73, https://doi.org/10.1038/s41575-018-0055-0.

[36] J. Tang, W. Peng, J. Ji, C. Peng, T. Wang, P. Yang, et al., GPR176 promotes cancer progression by interacting with G protein GNAS to restrain cell mitophagy in colorectal cancer, Adv. Sci. 10 (2023) e2205627, https://doi.org/10.1002/advs.202205627.

[37] M. Higashiyama, N. Motoi, M. Yotsukura, Y. Yoshida, K. Nakagawa, S. Yagishita, et al., Clinicopathological characteristics and molecular analysis of lung cancer associated with ciliated muconodular papillary tumor/bronchiolar adenoma, Pathol. Int. 73 (2023) 188–197, https://doi.org/10.1111/pin.13316.

[38] G.N. Dodoo, B. De, S.S. Lee, J. Abi Jaoude, J.N. Vauthey, C.D. Tzeng, et al., Brain metastases from biliary tract cancer: case series and clinicogenomic analysis, Oncol. 28 (2023) 327–332, https://doi.org/10.1093/oncolo/oyac273.

[39] X. Li, Q. Jin, Q. Yao, B. Xu, L. Li, S. Zhang, et al., The flavonoid quercetin ameliorates liver inflammation and fibrosis by regulating hepatic macrophages activation and polarization in mice, Front. Pharmacol. 9 (2018) 72, https://doi.org/10.3389/fphar.2018.00072.

[40] Y. Chen, T. Li, P. Tan, H. Shi, Y. Cheng, T. Cai, et al., Kaempferol from penthorum chinense pursh attenuates hepatic ischemia/reperfusion injury by suppressing oxidative stress and inflammation through activation of the Nrf2/HO-1 signaling pathway, Front. Pharmacol. 13 (2022) 857015, https://doi.org/10.3389/fphar.2022.857015.

[41] R. Jiang, P. Hao, G. Yu, C. Liu, C. Yu, Y. Huang, et al., Kaempferol protects chondrogenic ATDC5 cells against inflammatory injury triggered by lipopolysaccharide through down-regulating miR-146a, Int. Immunopharm. 69 (2019) 373–381, https://doi.org/10.1016/j.intimp.2019.02.014.

[42] J. Meng, Y. Li, F. Sun, W. Feng, H. Ye, T. Tian, et al., Salidroside alleviates LPS-induced liver injury and inflammation through SIRT1- NF-kappaB pathway and NLRP3 inflammasome, Iran J Basic Med Sci 27 (2024) 297–303, https://doi.org/10.22038/IJBMS.2023.69401.15124.

[43] X.N. Han, C.Y. Liu, Y.L. Liu, Q.M. Xu, X.R. Li, S.L. Yang, New triterpenoids and other constituents from the fruits of Benincasa hispida (Thunb.), Cogn, J Agric Food Chem. 61 (2013) 12692–12699, https://doi.org/10.1021/jf405384r.

[44] S. Zhu, H. Wen, W. Wang, Y. Chen, F. Han, W. Cai, Anti-hepatitis B virus activity of lithospermic acid, a polyphenol from Salvia miltiorrhiza, in vitro and in vivo by autophagy regulation, J. Ethnopharmacol. 302 (2023) 115896, https://doi.org/10.1016/j.jep.2022.115896.

[45] N.F. Abo El-Magd, D.H. El-Kashef, M. El-Sherbiny, S.M. Eraky, Hepatoprotective and cognitive-enhancing effects of hesperidin against thioacetamide-induced hepatic encephalopathy in rats, Life Sci. 313 (2023) 121280, https://doi.org/10.1016/j.lfs.2022.121280.

[46] A. Wu, H. Chen, C. Xu, J. Zhou, S. Chen, Y. Shi, et al., miR-203a is involved in HBx-induced inflammation by targeting Rap1a, Exp. Cell Res. 349 (2016) 191–197, https://doi.org/10.1016/j.yexcr.2016.10.016.

[47] W. Wang, Z. Chen, T. Zheng, M. Zhang, Xanthohumol alleviates T2DM-induced liver steatosis and fibrosis by mediating the NRF2/RAGE/NF-kappaB signaling pathway, Future Med. Chem. 13 (2021) 2069–2081, https://doi.org/10.4155/fmc-2021-0241.

[48] R. Das, V. Esposito, M. Abu-Abed, G.S. Anand, S.S. Taylor, G. Melacini, cAMP activation of PKA defines an ancient signaling mechanism, Proc Natl Acad Sci U S A. 104 (2007) 93–98, https://doi.org/10.1073/pnas.0609033103.

[49] S. Turan, M. Bastepe, GNAS spectrum of disorders, Curr. Osteoporos. Rep. 13 (2015) 146–158, https://doi.org/10.1007/s11914-015-0268-x.

[50] B. Liu, T. Sun, H. Li, S. Qiu, Y. Li, D. Zhang, Proximal tubular RAGE mediated the renal fibrosis in UUO model mice via upregulation of autophagy, Cell Death Dis. 13 (2022) 399, https://doi.org/10.1038/s41419-022-04856-z.

[51] F. Zheng, Q. Tang, X.H. Zheng, J. Wu, H. Huang, H. Zhang, et al., Inactivation of Stat3 and crosstalk of miRNA155-5p and FOXO3a contribute to the induction of IGFBP1 expression by beta-elemene in human lung cancer, Exp. Mol. Med. 50 (2018) 1–14, https://doi.org/10.1038/s12276-018-0146-6.

[52] A.M. Abdel-Moneim, M.A. Al-Kahtani, M.A. El-Kersh, M.A. Al-Omair, Free radical-scavenging, anti-inflammatory/anti-fibrotic and hepatoprotective actions of taurine and silymarin against CCl4 induced rat liver damage, PLoS One 10 (2015) e0144509, https://doi.org/10.1371/journal.pone.0144509.